Gamma prime formation in nickel-based superalloy IN738LC manufactured by laser powder bed fusion

Materials Today Communications 38 (2024) 107905

Contents lists available at ScienceDirect

Materials Today Communications

journal homepage: www.elsevier.com/locate/mtcomm

Gamma prime formation in nickel-based superalloy IN738LC manufactured by laser powder bed fusion

Fiona Schulz [a,b,*], Kristina Lindgren [c], Jinghao Xu [d], Eduard Hryha [a]

[a] Department of Industrial and Materials Science, Chalmers University of Technology, SE-41296, Göteborg
[b] Institute of Materials Science, Universität der Bundeswehr München, DE-85579 Neubiberg, Germany
[c] Department of Physics, Chalmers University of Technology, SE-41296, Göteborg
[d] Department of Management and Engineering, Linköping University, SE-58183 Linköping, Sweden

ARTICLE INFO

Keywords:
Laser powder bed fusion (LPBF)
IN738LC
Atom probe tomography (APT)
Gamma prime
Spinodal decomposition

ABSTRACT

Complex components for high-temperature gas turbine applications require materials that offer a combination of excellent high-temperature strength and oxidation resistance. Nickel-based superalloys with high gamma prime (γ) volume fractions are particularly suited for these applications, especially combined with additive manufacturing for intricate geometries. Despite the complex thermal history that these materials experience during laser powder bed fusion (LPBF) processing, γformation is suppressed when manufacturing IN738LC, which has a medium equilibrium γcontent of about 40–50 vol%. This study follows γformation in LPBF IN738LC during subsequent annealing treatments at temperatures ranging from 745 °C to 865 °C, creating an experimentally determined TTT (temperature-time-transformation) diagram. This diagram is largely based on scanning electron microscopy (SEM) imaging supported by Vickers hardness measurements and scanning transmission electron microscopy (STEM) bright field imaging. Atom probe tomography (APT) of the as-built material indicated nm-sized regions depleted in Cr and enriched in Ni, Al, and Ti, but show no characteristic superlattice patterns in TEM diffraction. APT and TEM diffraction analysis of material annealed at 850 °C for 3 min confirmed the presence of the γphase but indicated that γhad formed through spinodal decomposition instead of precipitation.

1. Introduction

Laser powder bed fusion (LPBF), newly termed powder bed fusion – laser beam (PBF-LB) according to ASTM standard 52900–2021, represents a complex thermal history with local melting of powder followed by extremely high cooling rates and intrinsic heat treatments during the manufacturing of subsequent layers [1]. LPBF of nickel-based superalloys is becoming increasingly interesting for manufacturing intricate parts designed for demanding applications. These materials are multi-component systems which comprise complex microstructures enabling their exceptional combination of material properties. Especially the coherent strengthening phase gamma prime (γ´) with an ordered $L1_2$ type structure contributes to the high strength of nickel-based superalloys [2]. The remarkable characteristic of the γ´phase is that an increase in volume fraction can be linked to an increasing yield strength at high temperatures [2,3].

Nickel-based superalloys with medium to high γ´content such as IN738LC (40–50 vol%) are considered as hard-to-weld alloys, representing great challenges during LPBF manufacturing, and are subject to current research [4–11]. The focus of most research is the presence of and mitigating strategies for crack formation of these alloys during and after processing. However, the complex thermal history of the LPBF process with high heating and cooling rates to and from the melt as well as intrinsic heat treatment cycles due to the layer-based process also has interesting implications on the resulting microstructure especially with respect to γ´particles.

The effects of LPBF manufacturing on the presence of these particles in nickel-based superalloys seem to depend on the respective alloy composition. The fast heating and cooling rates during the LPBF process seem to suppress γ´formation and even the intrinsic heat treatment owed to the layer-by-layer process does not allow for enough thermal energy for γ´ɒ form in IN738LC during the process [1,4,9,10,12,13]. But γ has been observed in the nickel-based superalloy CM247LC when analysing the as-built condition after LPBF manufacturing [11,13–15]. This

* Corresponding author at: Department of Industrial and Materials Science, Chalmers University of Technology, SE-41296, Göteborg.
E-mail address: fiona.schulz@mailbox.org (F. Schulz).

https://doi.org/10.1016/j.mtcomm.2023.107905
Received 30 August 2023; Received in revised form 3 December 2023; Accepted 17 December 2023
Available online 30 December 2023

Table 1
Elemental composition of as-built IN738LC determined by ICP-EOS and infrared absorption.

	Ni	Cr	Co	Al	Ti	W	Ta	Mo	Nb	Zr	B
wt%	61.0	15.5	8.8	3.3	3.7	2.9	1.8	1.9	0.9	0.03	0.01
at%	59.2	17.0	8.5	7.0	4.4	0.9	0.6	1.1	0.6	0.02	0.05
	Fe	Mn	P	Si	C	N	O	S			
wt%	0.04	< 0.005	< 0.003	0.03	0.091	0.00527	0.018	0.0017			
at%	0.04	< 0.01	< 0.01	0.06	0.4	0.02	0.07	0.003			

circumstance can be rationalised by the different alloy chemistry as well as the content of the γ´phase of both alloys; the equilibrium γ´content in IN738LC comprises 40–50 vol% while CM247LC contains ca. 60 vol%. Therefore, the driving force for precipitation should be higher in the latter alloy. This difference could be enough to account for the presence of γ´in as-built CM247LC and its absence in as-built IN738LC.

Classical γ´development is described as formation due to undercooling, driving nucleation bursts while cooling the material from above the γ´solvus temperature, and coarsening of already formed γ´particles at temperatures below the γ´solvus temperature. Accordingly, γ´particles precipitate when the local concentration of γ´formingelements (Al, Ti, Ta, Nb, Hf) is high and γ stabilizing elements (Cr, Co, Mo, W) are locally depleted [11,16–18]. Influencing factors for the resulting γ´precipitate number, shape and size distribution, are the applied cooling rate in addition to the content of γ´forming elements, the applied temperature and treatment duration as well as microstructural factors such as the lattice misfit between precipitate and [17,19–22]. For example, high cooling rates from γ´solvus have been shown to result in unimodal γ´size distributions with small particles sizes while slower cooling rates lead to multimodal size distributions with large as well as small particles [20,21].

However, the exact mechanism by which γ´forms from the γ matrix is debated in literature [23]. In continuous cooling studies with very high cooling rates, areas depleted in elements such as Cr, Co, or Mo and enriched in γ´forming elements such as Al and Ti were found but it was observed that these areas were interconnected [22–24]. This observation led to the suggestion that γ´precipitationinvolves a combination of a phase separation process such as spinodal decomposition and an ordering reaction [23,24]. To better understand the controlling formation mechanism of the γ´phase, Collins et al. [25] investigated nickel-based superalloy powder exposed to temperatures above and below γ´solvus with a combination of in-situ and ex-situ analysis methods. The authors observed γ formation via spinodal decomposition when investigating material during heating at temperatures below γ´solvus.

To fully exploit the advantages of LPBF of nickel-based superalloys, the as-built microstructure and its behaviour to subsequent processing needs to be better understood. The strengthening phase γ´is critical for the performance of nickel-based superalloys. As the LPBF process generates microstructures which significantly differ from material manufactured by conventional processes, it is likely that tailored heat treatment procedures are necessary [26–28]. As described above, the formation of γ´is not fully understood. Superalloys containing medium levels of γ´manufactured by LPBF are especially suitable to investigate γ´formation mechanisms due to the fast heating and cooling rates resulting in supersaturated matrix material without fully formed γ´particles[1,4,13,29].

For this reason, the material chosen for this current study was IN738LC manufactured by LPBF. The manufactured material was systematically exposed to annealing temperatures below the γ´solvus temperature for increasing length of time to experimentally determine a TTT diagram for γ´formation. Scanning electron microscopy of the as-built and annealed material was supported by scanning transmission electron microscopy and Vickers hardness measurements to identify the strengthening effects through the presence of the γ´phase. Atom probe tomography of as-built IN738LC and a targeted annealed sample was carried out to elucidate γ´formation in detail. For this analysis, particular emphasis is placed in Al and Ti as γ forming elements as well as Cr and Co for γ stabilising elements.

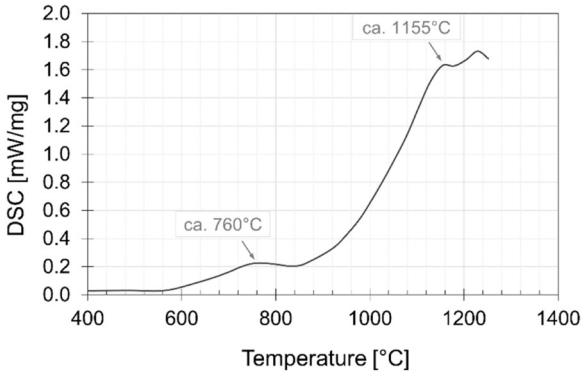

Fig. 1. DSC analysis of as-built IN738LC. Changes in enthalpy corresponding to ~760 °C and ~1155 °C are considered to correspond the γ´formation and the γ´solvus temperature, respectively. The change in enthalpy at ~1235 °C is correlated to the formation of carbides. For subsequent annealing treatments, 760 °C is taken as the starting point.

2. Material and methods

IN738LC samples were manufactured using an EOS M290 machine equipped with an Yb-fibre laser of a nominal maximum power 400 W. The parameters comprised 210 W laser power, 1750 mm/s laser scanning speed, 0.05 mm hatch distance, 0.02 mm layer thickness, and 67° scan rotation after each layer. The feed-stock material was gas atomized powder with the standard IN738LC composition (see below) supplied by EOS Finland OY with a typical particle size range of 25–63 μm. Cubes for microstructural analysis and heat treatments with dimensions of 5 mm × 5 mm x 10 mm were manufactured directly onto a substrate plate and later separated using wire electrical discharge machining resulting in final sample dimensions of 5 mm × 5 mm x 8 mm.

The elemental composition of the as-built material was analysed and is shown in Table 1. All metallic alloying elements were measured by induction coupled plasma optical emission spectroscopy (ICP-EOS) on a Spectro Arcos (Spectro Analytical Instruments GmbH, Germany), C and S were measured by infrared absorption after combustion in an induction furnace on a LECO CS844 (LECO Corporation, USA), and O as well as N were analysed by inert gas fusion on a LECO ON836 elemental analyzer.

Temperatures of interest during the heating period of post-manufacturing heat treatments were determined by differential scanning calorimetry (DSC) measurement using a heating rate of 10 K/min from room temperature to 1250 °C with 10 min hold at the maximum temperature (see Fig. 1). As DSC sample, the topmost 2 mm section of a 15 mm long rod with a diameter of 2 mm built alongside the microstructure cubes was cut using a standard abrasive saw.

Annealing treatments between 745 °C and 865 °C were applied in air using a ceramic tube furnace to investigate γ´formation during heating of as-built IN738LC manufactured by LPBF. For each annealing treatment, three cubes were laid on a single ceramic boat and inserted into

Table 2
Annealing matrix for LPBF IN738LC. The annealing matrix was first extended with temperatures 805 °C and 835 °C. Based on the results, a second extension to 850 °C and 865 °C was applied. Additionally, annealing treatments at 820 °C with corresponding exposure times to the highest temperatures were carried out.

Annealing temperature	Annealing time in minutes					
745 °C	1,			10,	100,	1000
775 °C	1,			10,	100,	1000
805 °C	1,			10,	100,	
820 °C		3,	5,			
835 °C	1,			10,	100,	
850 °C	1,	3,	5,			
865 °C	1,	3,	5,			

the hot furnace. Once placed in the hot zone of the furnace, the tube was closed to minimize heat fluctuations and a timer was started for each set. Calculations of the heating time for a sample can be found in the supplementary material. Upon reaching the annealing time, the ceramic boat was quickly pulled out of the tube furnace and quenched in water.

Based on the DSC results, 760 °C was taken as an initial temperature of interest and annealing treatments were performed at both below and above this temperature (745 °C and 775 °C, respectively). The temperature matrix was then extended as detailed in Table 2.

The annealed cubes were cut parallel to the building direction, mounted in conductive Bakelite, prepared metallographically to ¼ μm finish und subsequently etched to reveal precipitates. The material was etched chemically using Marble's reagent for 10–30 s. SEM analysis was carried out on a Zeiss LEO Gemini 1550 FEGSEM equipped with an InLens detector. Vickers hardness was measured with a DuraScan G5 system on mounted and polished samples annealed at both 850 °C and 865 °C with a load of 0.3 kg. The hardness value given for each sample is the average of a 4 × 4 indent matrix with 0.5 mm interspacing (greater than 10x the indent size with approx. 35 μm). For reference, Vickers hardness of the as-built material was measured using the same settings on a Q60A+ EVO hardness tester (ATM Qness GmbH).

STEM samples were prepared using the twin-jet method; following grinding, TEM foils were polished down to 60–80 μm and final polishing was performed on a Struers twin-jet electropolisher. The electrolyte solution comprised 90% ethanol and 10% perchloric acid. The polishing voltage was set to 20 kV, and the polishing temperature was − 25 °C.

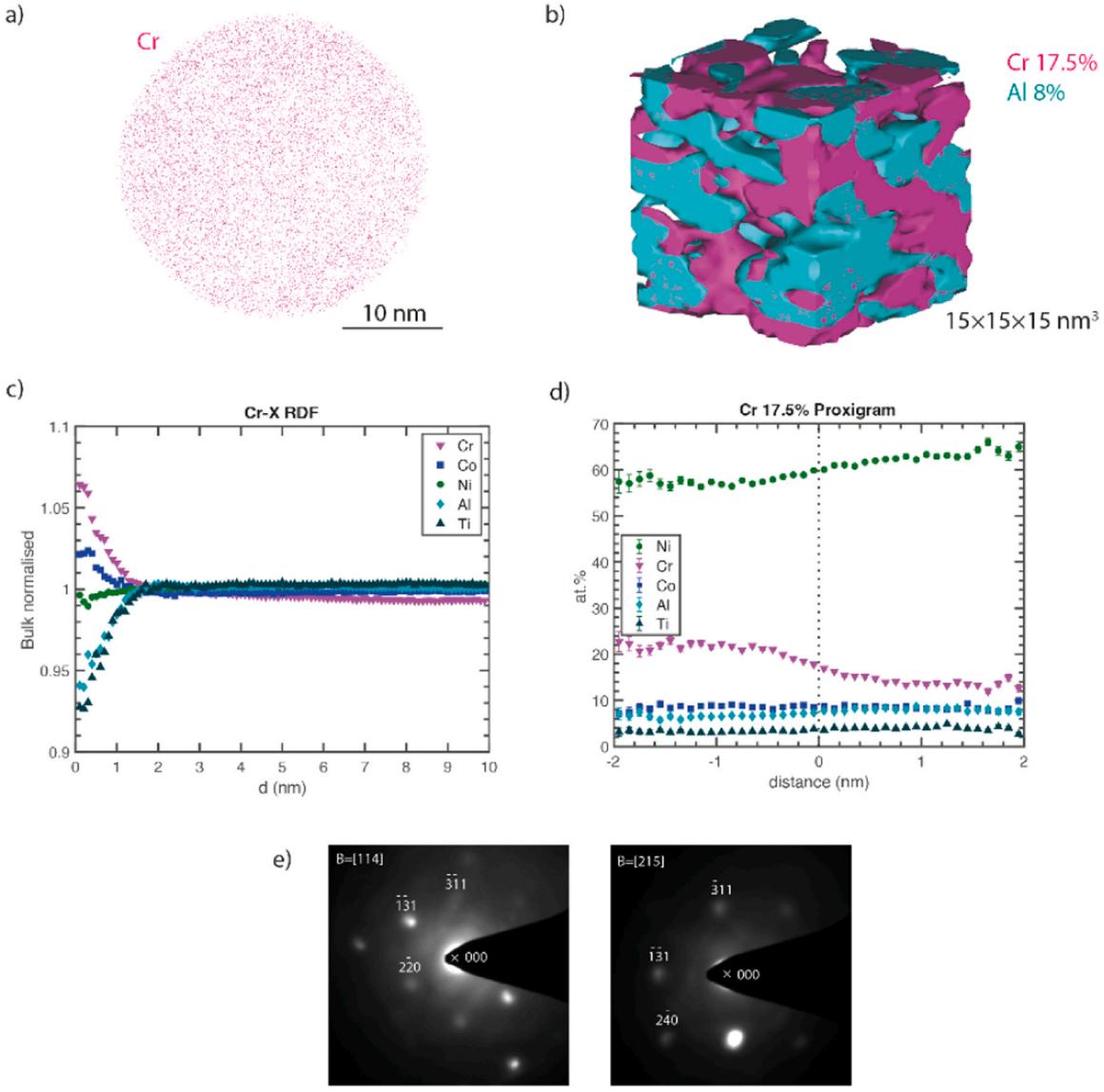

Fig. 2. APT data and TEM diffraction on as-built IN738LC. In a) the Cr atoms in a 5 nm thick slice of the APT reconstruction is shown. In b) a cube of the APT reconstruction with the side of 15 nm is shown. Isoconcentration surfaces of 17.5% Cr and 8% Al illustrate an early stage of phase separation. In c), the Cr-X RDFs for X = Cr, Co, Ni, Al, and Ti are shown. The proxigram of the Cr 17.5% isosurfaces is shown in d). e) shows TEM diffraction of the as-built material.

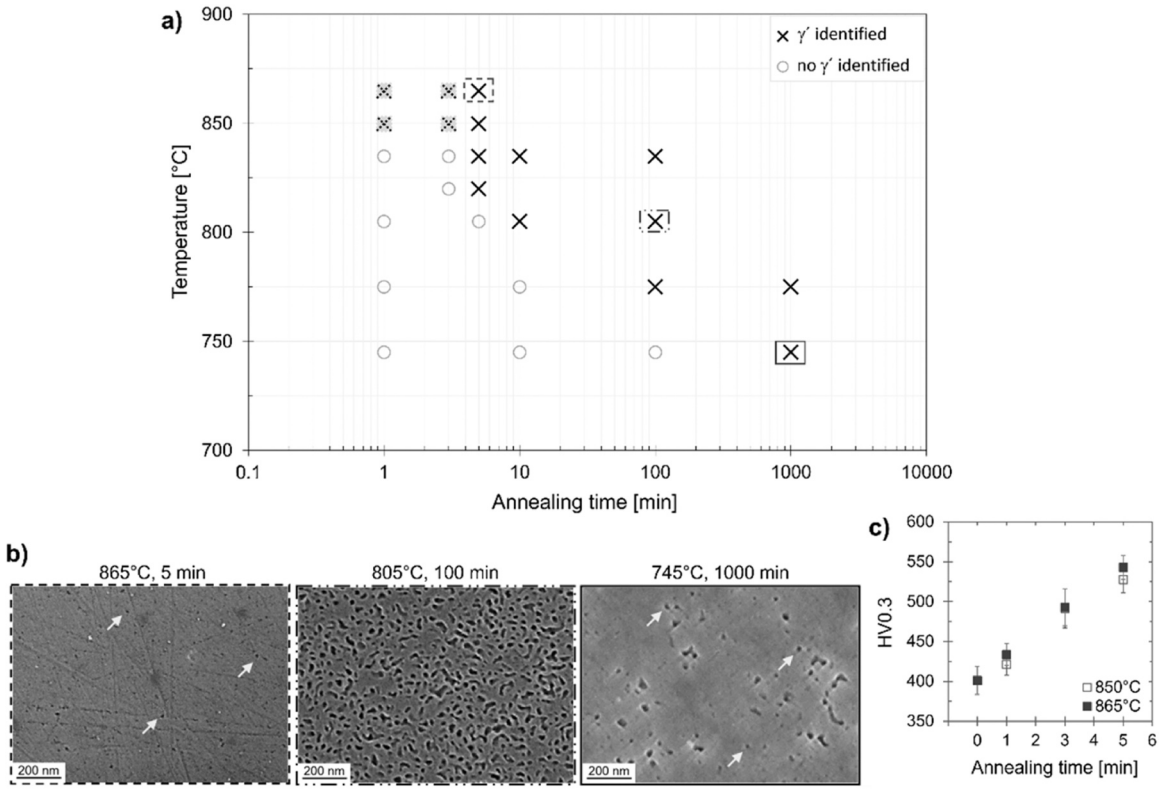

Fig. 3. Experimentally determined TTT diagram for the γ´formation in IN738LC manufactured by LPBF. The TTT diagram in a) is based on combined SEM and hardness measurement analysis performed on material annealed at temperatures ranging from 745 °C to 865 °C. Data points with light grey filling at 850 °C and 865 °C, respectively, are based on Vickers hardness results. The SEM images shown in b) display γ´particles at different stages of formation with respect to annealing temperature and time. In c) complementary results of hardness measurements of material annealed at 850 °C and 865 °C are shown. These results aided the generation of the TTT diagram as the γ´particles became too small for observation by SEM. The error bars represent the standard deviation.

Bright field STEM micrographs were taken on an FEI Tecnai G2 microscope running at 200 kV accelerating voltage with a camera length of 2100 mm.

Specimens for APT were prepared by a standard two-step electropolishing procedure [30], finished with some microsecond pulses. The specimens were analysed in a AMETEK Cameca LEAP 3000X HR, with 20% pulse fraction, a pulse frequency of 200 kHz, and a temperature of 50–70 K.

Both STEM and APT analysis were conducted on material taken from the bulk of the samples.

The APT data was reconstructed and analysed in IVAS 3.6. For the reconstruction, the evaporation field was set to 35 V/nm and the image correction factor to 1.65. For the specimen heat treated at 850 ° for 3 min, the radial distribution functions (RDFs) were used to calibrate the k value, using a methodology described in [31]. This method uses the RDF of an element that is involved in spinodal decomposition. By varying k and comparing the RDFs, a k where the extent of spinodal decomposition is similar in all (x, y, and z of the analysis) directions can be chosen. For the analyses in this paper, $k = 4.9$ and $k = 5.1$ were found to be optimal for the two different analyses. All RDFs can be seen in the supplementary material, Fig. S1 and S2. For the as-built material, $k = 5.0$ was used. The amplitude of the spinodal decomposition was evaluated using the RDF-method by Zhou et al. [32]. The wavelength was estimated as the first local maximum of the Cr-Cr RDF.

TEM diffraction was performed on electropolished APT specimen (for as-built material), and on a lift out lamella (for material heat treated at 850 °C for 3 min). The lamella was prepared in a FEI Versa 3D FIB/SEM and finalised with a 5 kV mill to remove amorphous material on the surface. TEM diffraction was carried out on an FEI Tecnai, operated at 200 kV. The APT specimen could only be tilted in one direction in the TEM due to the shape of the specimen (needle). For the lamella, a standard double tilt holder was used.

3. Results

As-built IN738LC does not contain any γ´precipitates according to the APT data in Fig. 2. However, the APT results show Cr-depleted volumes throughout the material. Additionally, these volumes are slightly enriched in Al and Ti. These areas, also identified in a previous study on a variant of IN738LC [29], were initially hypothesized to be γ´precursors. Considering the Cr atoms seen in the slice in a) are close to evenly distributed, the volumes enriched in Al and Ti are much smaller than 10 nm. In b), isoconcentration surfaces show that the volumes of high Cr are interconnected rather than separate precipitates. The extent of the uneven Cr distribution is illustrated in the RDF in c). Cr atoms tend to be close to other Cr atoms and to Co, but further away from Ni, Al and Ti. The same tendency can be seen in the proxigram for Cr 17.5% isoconcentration surfaces, in d). In the TEM diffraction patterns in e), no superlattice reflections could be seen. Thus, there is no significant ordering in the γ´precursors in the as-built material. Split proxigrams for d) separating low-content elements (Co, Al, Ti) can be seen in the supplementary material Fig. S3. The dotted line in the proxigram indicates the change in Cr-concentration, marking a representative isoconcentration surface as shown in b).

Based on qualitative SEM analysis of the annealed samples etched using Marble's reagent, an experimental TTT could be established as shown in Fig. 3. The chemical etchant removed the ordered γ´phase which then appears as dark areas on SE images as representatively shown in Fig. 3b). When exposing as-built material to 745 °C, γ´particles could only be identified after 1000 min exposure, while γ´particles could be identified as early as 5 min at 865 °C. Identification of the γ´particles was possible with reference to as-built material

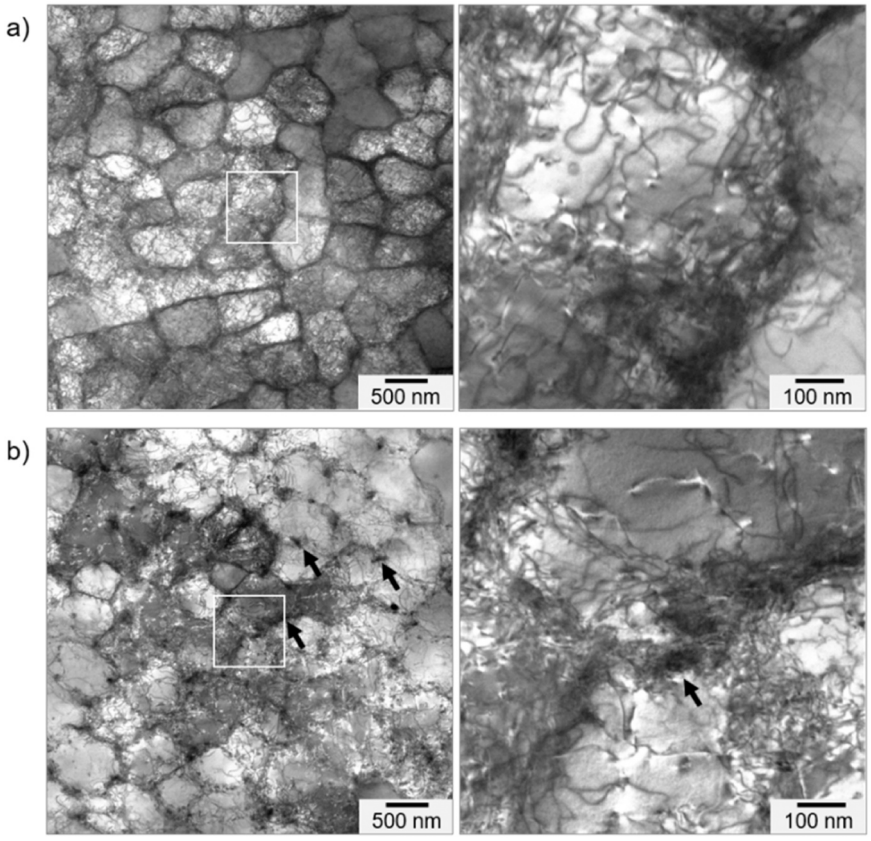

Fig. 4. TEM bright field images of IN738LC annealed at 865 °C for a) 1 min, and b) 3 min. High dislocation density is observed inside the individual cells for both conditions. After annealing at 865 °C for 3 min, particles are observed, indicated by the black arrows. Identification of γ´particles, however, is not possible.

subjected to the same etching conditions and in conjunction with the results of complementary analysis described below. Contrary to investigations into γ´formation during cooling from super-solvus temperatures, no nucleation bursts from supercooling occurs which makes γ´formation in this experiment diffusion-controlled from a supersaturated matrix similar to the results presented by Collins et al. [25]. This is consistent with the relationship between annealing temperature vs annealing time with γ´particles being detectable after shorter times at higher temperatures. SEM analysis showed different γ´morphologies at different temperatures as demonstrated in Fig. 3b). Both the material annealed at 745 °C for 1000 min and the one annealed at 865 °C for 5 min display discrete areas of γ´which appear like individual particles. The material annealed at 805 °C for 100 min, however, displays a seemingly interconnected γ´phase with irregular shapes as shown in Fig. 3b), comparable to the ones reported by [23] and [22].

While the chemical etchant removes the γ´phase and is therefore less prone to over-etching effects, the detection of γ´particles remains challenging with low γ´phase content and small particle sizes. As an increase in γ´particles can be linked to an increase in the alloy's hardness, the TTT diagram is supplemented by hardness measurements for the material heat treated at 850 °C and 865 °C to aid indication of γ´(see Fig. 3c)). Compared to the hardness of as-built IN738LC (401 HV0.3), a slight increase in hardness can be observed after as little as 1 min annealing at 850 °C. This increase in hardness is more distinct when the material is annealed at 865 °C where the error bars of the annealed material do not overlap with the error bars of the as-built material, suggesting γ´started to form. A significant increase in hardness values can be observed for both samples annealed for 3 min and 5 min, respectively. After 5 min, γ´precipitates could be detected via SEM.

STEM bright field images in Fig. 4 show a high density of dislocations in the material annealed at 865 °C for both 1 min and 3 min. The contrast of the dense dislocations inhibits the identification of γ´particles since the local cell boundaries seem to be preferred areas for dislocation accumulation as well as γ´or secondary phase formation. After 3 min annealing at 865 °C particles can be identified (indicated by black arrows in Fig. 4b)).

Electron diffraction patterns and corresponding TEM bright field micrographs of IN738LC annealed at 865 °C for 1 min and 3 min, respectively, were recorded as shown in Fig. 5. Despite the strong contrast from the strain field owing to the presence of dense dislocations, cellular structures with sub-micron size are identified. For both material conditions, $L1_2$ γ´superlattice reflections can be observed (indexed in yellow). The material exposed to 865 °C for 3 min displays a (qualitatively) higher intensity of the superlattice reflections. Some local dislocation recovery can be identified as highlighted by the arrow in Fig. 5b).

The material heat treated at 850 °C for 3 min contains γ´, as seen in the APT results displayed in Fig. 6. A 5 nm thick slice through the dataset shows clear phase separation of Cr in Fig. 6a). The three-dimensional nature of the phase separation can be seen in b), suggesting that this is spinodal decomposition rather than precipitation of γ´. The RDF and proxigram confirm the formation of a Cr-rich γ and a Ni_3(Al,Ti) γ´phase being present in the material. Further analysis of the RDFs gives a spinodal wavelength (estimated as the first local maxima of the Cr-Cr RDF) of 6.8–8.2 nm and amplitude of 9.9–12.4%, where the interval is describing the difference between the two APT analyses in the different local volumes. TEM diffraction reveals superlattice reflections, indicating the presence of ordering in γ´. As before, split proxigrams for d) separating low-content elements (Co, Al, Ti) can be seen in the supplementary material Fig. S3.

4. Discussion

The as-built IN738LC material contained no γ´phase as shown by

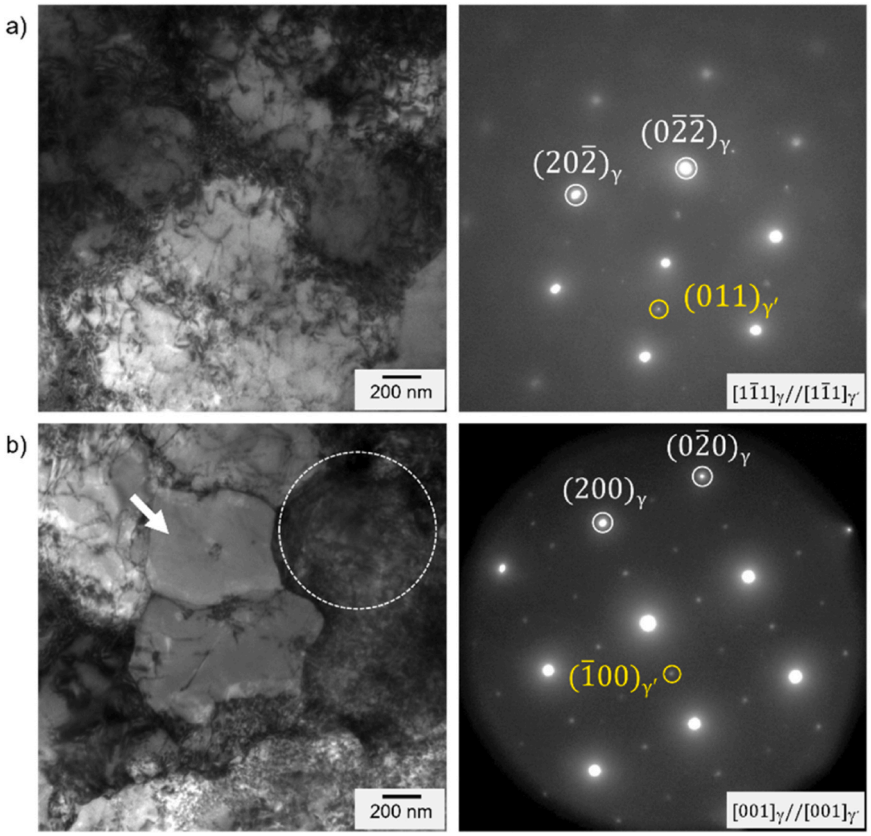

Fig. 5. TEM bright field micrographs and corresponding electron diffraction patterns for IN738LC annealed at 865 °C for a) 1 min and b) 3 min. $L1_2$ γ´superlattice reflections are indexed in yellow.

TEM diffraction analysis (Fig. 2) which confirmed findings elsewhere in literature investigating the same material [1,4,12] as well as the results of a previous study on an IN738LC variant [29]. Based on the DSC results (see Fig. 1), first annealing treatments were carried out at 745 °C and 775 °C, respectively. While these temperatures are lower than the annealing temperature according to the standard heat treatment for this alloy [33], it was thought that the severe non-equilibrium states caused by the fast heating and cooling rates during the LPBF process could facilitate faster γ´formation thus justifying annealing treatments at these temperatures. Results from the previous study seemed to support this hypothesis as APT analysis indicated Cr-depleted/Al-enriched regions which were thought to be γ´precursors [29].

The γ´-precursor hypothesis needed to be revised upon seeing the APT results of the material annealed at 850 °C for 3 min. TEM diffraction confirmed that γ´had formed but APT analysis showed that this did not occur through particle formation but spinodal decomposition (Fig. 6). As mentioned in the introduction, the exact γ´formation mechanism is a point of recurring scientific investigation and discussion [23–25]. Collins et al. [25] investigated powder of a nickel-based superalloy by applying heat treatments below the alloy's γ´solvus temperature and identified spinodal decomposition as γ´formation. This formation step has previously also been reported by Tan et al. [23] and Viswanathan et al. [24]. The work by Collins et al. is particularly interesting to the current study as powder is the feedstock material for the LPBF process and, as with atomization, the heating and cooling rates deviate significantly from standard manufacturing processes for which γ´formation has been studied extensively [17,19–22].

The present study focuses on heating the material from room temperature instead of observing cooling dynamics coming from high temperatures. This focus on heating means that no undercooling takes place in the material, further supporting the hypothesis of γ´formation through spinodal decomposition [23,25]. Collins et al. [25] hypothesised that the matrix material undergoes phase separation via spinodal decomposition by forming small domains depleted in γ forming elements like Cr and enriched in γ´forming elements such as Al. This hypothesis corresponds to the precursor areas depleted in Cr which were observed in as-built IN738LC (see Fig. 2) and has also been reported by Tan et al. [23] who investigated γ´precipitation kinetics in a single crystal nickel-based alloy. The isoconcentration surfaces from the APT analysis (see Fig. 6) support the idea of spinodal decomposition instead of classic precipitation in the early stages of formation. The shape of the emerging γ´phase with its interconnected characteristic is also distinctly different from nuclei that would be expected when classic precipitation occurs. However, discrete γ´particles are observed for several of the annealing conditions (compare Fig. 3b)) which suggests that spinodal decomposition is likely a factor but does not describe the full extent of γ´formation. This suggests that γ´formation in LPBF IN738LC involves a combination of a phase formation processes as suggested in literature for other commercial superalloys [18,23,24]. It is plausible to assume a formation sequence as suggested by Tan et al. [23] whereby γ´forms first through spinodal decomposition until the discrete areas of γ´reach a critical size after which the mechanisms of particle growth according to nucleation theory prevails which leads to the familiar γ´particle structure characteristic of all heat-treated nickel-based superalloys. Interestingly, Adegoke et al. [11] recently reported similar Cr-partitioning behaviour in CM247LC but noted that this remained limited to Cr only, leading to the suggestion that a meta-stable Cr-rich phase forms in the alloy instead. While Cr displays the strongest partitioning behaviour in IN738LC in the current study, a corresponding change in Al-content is observed (see Fig. 6d)) which could indicate that the exact process of γ´formation might differ between IN738LC and CM247LC.

That γ´particles can be detected in as-built condition for alloys with high volume contents of γ´would not contradict this theory: Alloys

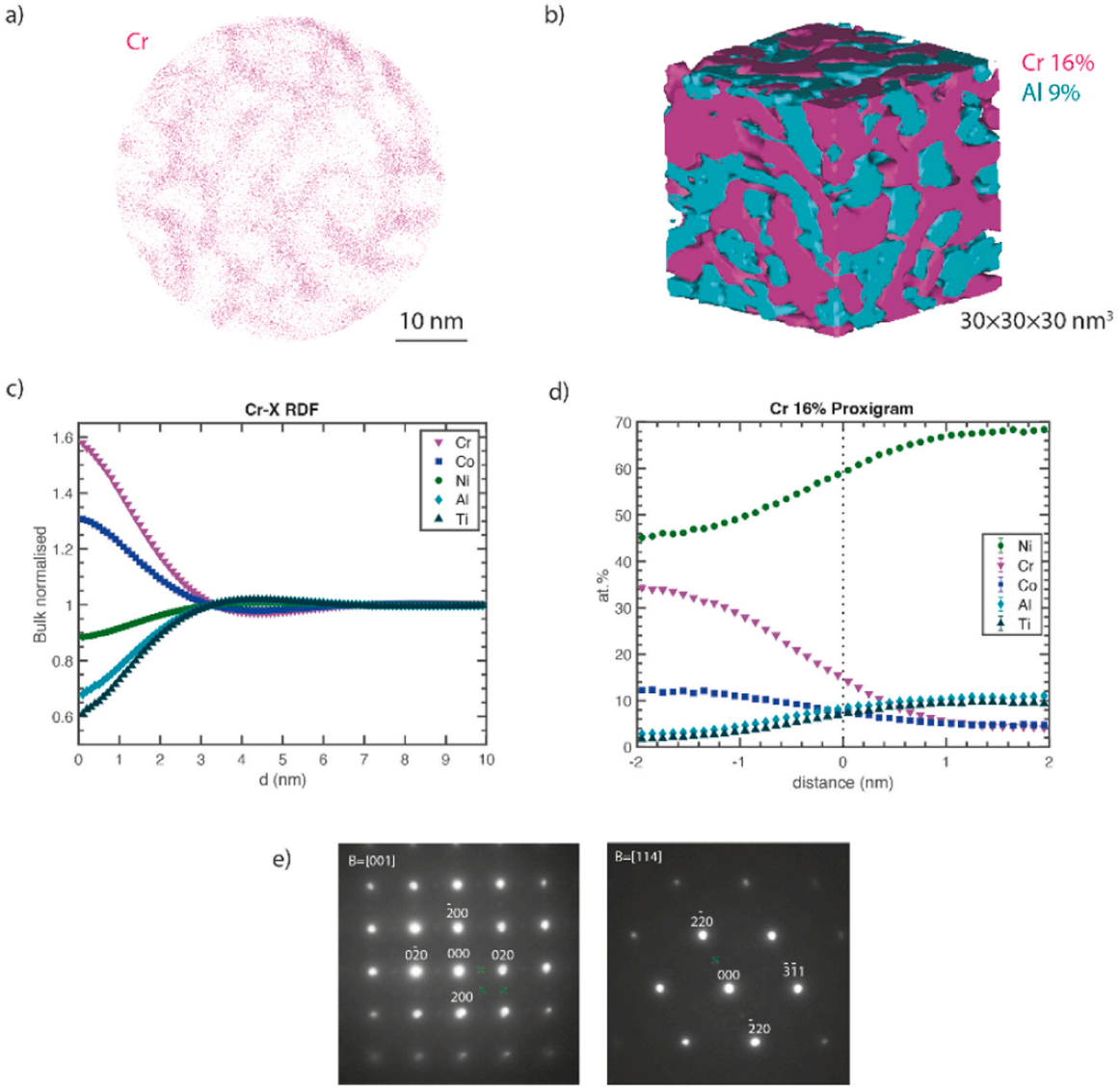

Fig. 6. APT data and TEM diffraction of the material annealed at 850 °C for 3 min. In a) the Cr atoms in a 5 nm thick slice of the APT reconstruction are shown. In b) a cube of the APT reconstruction with the side of 30 nm is shown. Isoconcentration surfaces of 16% Cr and 9% Al illustrate a phase separation. In c), the Cr-X RDFs for X = Cr, Co, Ni, Al, and Ti are shown. The proxigram of the Cr 16% isosurfaces are shown in d). e) shows TEM diffraction of the material annealed at 850 °C for 3 min. Superlattice reflections are marked with green crosses.

containing high amounts of γ´, such as CM247LC, consequently contain higher amounts of γ´forming elements which result in a stronger driving force within the material to form γ´particles. Since the layer-wise process of LPBF comprises intrinsic heat treatment steps following the initial melting, the total time required at temperatures high enough to facilitate γ´formation would then be sufficiently long for these alloys while not quite long enough for alloys with lower γ´volume fraction such as IN738LC. That discrete γ´particles are observed in as-built CM247LC would also not conclusively prove that only conventional nucleation theory applies since the spinodal decomposition phase may be so brief that both spinodal decomposition and particle growth occur during intrinsic heat treatment.

It is, of course, interesting to compare the experimentally determined TTT diagram for γ´formation of this study with computational diagrams as shown in Fig. 7 and described in literature [5]. At first glance, it becomes apparent that the annealing temperatures chosen for the current study are comparatively low while the annealing times are comparatively long. However, the experimental setup would be insufficient to investigate shorter annealing times which would be required at higher annealing temperatures. It is interesting to note, however, that while computational TTT diagrams predict complete γ´formation within seconds at 850 °C, APT analysis of the annealed material (3 min/850 °C) clearly showed that while γ´occurred, it was not present in the form of particles.

On the other hand, it should be considered that the experimentally determined TTT diagram required complementary analysis such as Vickers hardness measurements and selected STEM and APT analysis. While an increase in hardness is a good indicator for the presence of γ´, it is no definite determinant of the strengthening phase. STEM bright field micrographs show no indication of γ´formation through spinodal decomposition, but the overlaps caused by the thickness of the TEM foil makes identification of the strengthening phase difficult. STEM analysis does, however, indicate that γ´forms at the cell boundaries as discrete particles (see Fig. 4) and TEM diffraction analysis presents a higher intensity of the $L1_2$ superlattice reflections for the material with longer annealing time (see Fig. 5). Interestingly, the diffraction pattern shown here was recorded from the circled area with a high density of dislocations indicating that dislocation recovery is not a prerequisite for

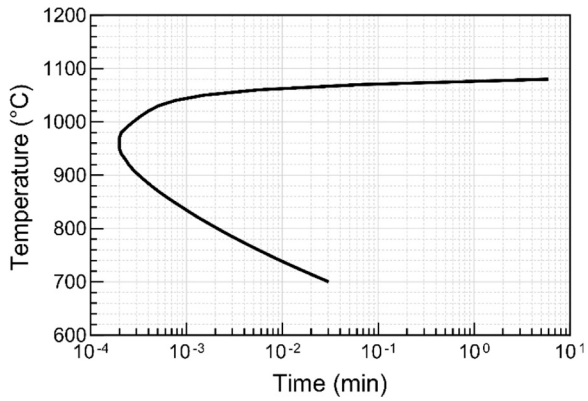

Fig. 7. Simulated TTT diagram representing 10% γ´formation in the γ matrix in the manner of bulk nucleation. To simplify the calculation, only Cr, Co, Mo, W, Al, Ti, Ta, and Nb were included to simulate this diagram. TC Prisma input parameters comprised matrix (FCC_L12, disregard el. properties, grain size 50 μm, aspect ratio 10, dis. density 2E14), precipitate (FCC_L12#2, nucleation calculated from bulk, calculated pre-factor for interfacial energy 1, simplified growth rate model, spherical morphology, phase boundary mobility 10, phase energy addition 0), temperature (700–1200 °C), annealing times (max. 1000 min).

γ´formation. SEM images taken of the material annealed at 865 °C for 5 min further indicates the presence of individual γ´particles (see Fig. 3b)). However, in the case of the SEM micrograph, the complementary analysis was necessary to interpret the observed particles as γ´. Both STEM and SEM could be taken as indicator that γ´formation occurs through a combination of spinodal decomposition followed by particle formation at preferential sites like cell boundaries before particles form everywhere. Such a mix of formation events is further supported by SEM images taken of the material annealed at 805 °C for 100 min and at 745 °C for 1000 min (compare Fig. 3b)) as well as results presented in literature which display γ´as interconnected areas characteristic of spinodal decomposition [18,22–24]. Of course, formation kinetics of the γ´phase are dependent on multiple factors, not least the overall content of γ´forming elements in the alloy [5]. While computational models predict very rapid γ´formation during annealing, annealing experiments of rapidly quenched nickel-based superalloys indicate slower formation kinetics [18,34].

Understanding the formation sequence and growth kinetics of the γ´phase is critical to derive tailored heat treatment procedures to achieve advantageous mechanical properties [35]. The presence of γ´in nickel-based superalloys is not only essential for their mechanical performance but also oxidation and corrosion properties. It is clear from the literature and data presented that γ´formation in nickel-based superalloys leaves room for debate. Due to the inherently fast heating and cooling rates of the LPBF process and the medium γ´content in IN738LC, γ´formation is suppressed during manufacturing, leaving the material just at the edge of γ´formation in the as-built condition. Based on the presented findings, heat treatment procedures could be derived to tailor γ´formation. For one, super-solvus heat treatment steps are not necessary from a γ´formation point of view since no γ´is present in the as-manufactured material, eliminating the need to dissolve any precipitated γ´particles. The super-saturated material matrix in the as-built state likely leads to uniform size distributions of γ´. To achieve bi- or multi-modal γ´size distributions, sub-solvus heat treatment procedures could be explored. Aspects such as grain size or carbides play another significant role in the mechanical performance of nickel-based superalloys and may require adjustments of heat treatment procedures, however, the interplay with and trade-off in γ´size and distribution may need different approaches than conventional heat treatment cycles above and below γ´solvus for extended amounts of time.

One approach to tailor the γ´phase could be additive manufacturing itself, where a better understanding of the γ´formation could be leveraged by employing specific manufacturing parameters to achieve the presence of different γ´distributions. The circumstance of γ´suppression in IN738LC during LPBF manufacturing offers an advantageous insight into the γ´formation mechanism, considering that precipitation events during continuous cooling in classical γ´development theory is attributed to local supersaturation of γ´forming elements. The presented findings should therefore be particularly useful to LPBF nickel-based superalloys but also applicable beyond LPBF material.

5. Conclusions

This study, investigating as-built and subsequently annealed IN738LC by using SEM, TEM, and APT analysis presents these key findings:

- The results of both APT and SEM analysis suggest a combination of a γ´formation processes involving spinodal decomposition in LPBF IN738LC.
- APT and TEM diffraction analysis confirmed that no γ´phase is present in IN738LC manufactured by LPBF in its as-built condition. Cr-depleted zones were found which displayed increased amounts of Ni, Al, and Ti, however, no superlattice diffraction, suggesting γ´-precursors instead of fully formed γ´.
- The γ´phase forms during annealing treatments at temperatures (745 °C – 865 °C) well below γ´solvus (approx. 1155 °C). The formation of γ´was summarized in an experimentally determined TTT diagram for LPBF IN738LC based on qualitative SEM analysis and complementary hardness measurements as well as electron diffraction.
- APT analysis of the material annealed at 850 °C for 3 min revealed that γ´formed with a morphology suggesting spinodal decomposition instead of classically assumed precipitation. The patterns of the precursors observed in as-built condition and the γ´phase present at different annealing conditions confirm γ´formation via spinodal decomposition.

CRediT authorship contribution statement

Hryha Eduard: Conceptualization, Funding acquisition, Project administration, Writing – review & editing. **Xu Jinghao:** Formal analysis, Investigation, Methodology, Visualization, Writing – review & editing. **Lindgren Kristina:** Conceptualization, Formal analysis, Investigation, Methodology, Visualization, Writing – review & editing. **Schulz Fiona:** Conceptualization, Formal analysis, Investigation, Methodology, Visualization, Writing – original draft, Writing – review & editing.

Declaration of Competing Interest

The authors declare that they have no known competing financial interests or personal relationships that could have appeared to influence the work reported in this paper.

Data availability

Data will be made available on request.

Acknowledgements

This work has been performed in the framework of the project “Materials for green hydrogen fueled gas turbines through additive manufacturing (MAGDA)” and the Centre for Additive Manufacturing – Metal (CAM^2), all supported by the Swedish Governmental Agency of Innovation Systems (Vinnova). Support from the Area of Advance Production at Chalmers are also acknowledged. The APT and TEM was

performed in the Chalmers Materials Analysis Laboratory (CMAL). Olof Bäcke is acknowledged for support with the TEM and Mattias Thuvander and Krystyna Stiller for fruitful discussions. Swathi Kiranmayee Manchili is acknowledged for her support in carrying out the DSC measurement. The chemical analysis of the as-built material was carried out by Dmitri Riabov at Höganäs AB.

Appendix A. Supporting information

Supplementary data associated with this article can be found in the online version at doi:10.1016/j.mtcomm.2023.107905.

References

[1] E.A. Jägle, Z. Sheng, L. Wu, L. Lu, J. Risse, A. Weisheit, et al., Precipitation reactions in age-hardenable alloys during laser additive manufacturing, JOM 68 (3) (2016) 943–949, https://doi.org/10.1007/s11837-015-1764-2.
[2] C.T. Sims, N.S. Stoloff, W.C. Hagel, I.I. Superalloys, in: Chester T. Sims, Norman S. Stoloff, William C. Hagel (Eds.), High-temperature materials for aerospace and industrial power, Wiley, New York, Chichester, 1987.
[3] P. Beardmore, R.G. Davies, T. Johnston, On the temperature dependence of the flow stress of nickel-base alloys, Trans. Metall. Soc. AIME 245 (1969) 1537–1545.
[4] A. Després, C. Mayer, M. Veron, E.F. Rauch, M. Bugnet, J.-J. Blandin, et al., On the variety and formation sequence of second-phase particles in nickel-based superalloys fabricated by laser powder bed fusion, Materialia 15 (2021) 101037, https://doi.org/10.1016/j.mtla.2021.101037.
[5] O. Adegoke, J. Andersson, H. Brodin, R. Pederson, Review of laser powder bed fusion of gamma-prime-strengthened nickel-based superalloys, Metals 10 (8) (2020) 996, https://doi.org/10.3390/met10080996.
[6] R. Engeli, T. Etter, S. Hövel, K. Wegener, Processability of different IN738LC powder batches by selective laser melting, J. Mater. Process. Technol. 229 (2016) 484–491, https://doi.org/10.1016/j.jmatprotec.2015.09.046.
[7] M. Cloots, P.J. Uggowitzer, K. Wegener, Investigations on the microstructure and crack formation of IN738LC samples processed by selective laser melting using Gaussian and doughnut profiles, Mater. Des. 89 (2016) 770–784, https://doi.org/10.1016/j.matdes.2015.10.027.
[8] A. Luca, de, C. Kenel, S. Griffiths, S.S. Joglekar, C. Leinenbach, D.C. Dunand, Microstructure and defects in a Ni-Cr-Al-Ti γ/γ' model superalloy processed by laser powder bed fusion, Mater. Des. 201 (2021) 109531, https://doi.org/10.1016/j.matdes.2021.109531.
[9] J.A. Muñiz-Lerma, Y. Tian, X. Wang, R. Gauvin, M. Brochu, Microstructure evolution of Inconel 738 fabricated by pulsed laser powder bed fusion, Prog. Addit. Manuf. 4 (2) (2019) 97–107, https://doi.org/10.1007/s40964-018-0062-2.
[10] S.E. Atabay, O. Sanchez-Mata, J.A. Muñiz-Lerma, R. Gauvin, M. Brochu, Microstructure and mechanical properties of rene 41 alloy manufactured by laser powder bed fusion, Mater. Sci. Eng.: A 773 (2020) 138849, https://doi.org/10.1016/j.msea.2019.138849.
[11] O. Adegoke, C. Kumara, M. Thuvander, F. Deirmina, J. Andersson, H. Brodin, et al., Scanning electron microscopy and atom probe tomography characterization of laser powder bed fusion precipitation strengthening nickel-based superalloy, Micron 171 (2023) 103472, https://doi.org/10.1016/j.micron.2023.103472.
[12] K. Kunze, T. Etter, J. Grässlin, V. Shklover, Texture, anisotropy in microstructure and mechanical properties of IN738LC alloy processed by selective laser melting (SLM), Mater. Sci. Eng.: A 620 (2015) 213–222, https://doi.org/10.1016/j.msea.2014.10.003.
[13] M.P. Haines, V.V. Rielli, S. Primig, N. Haghdadi, Powder bed fusion additive manufacturing of Ni-based superalloys: a review of the main microstructural constituents and characterization techniques, J. Mater. Sci. 57 (30) (2022) 14135–14187, https://doi.org/10.1007/s10853-022-07501-4.
[14] V.D. Divya, R. Muñoz-Moreno, O. Messé, J.S. Barnard, S. Baker, T. Illston, et al., Microstructure of selective laser melted CM247LC nickel-based superalloy and its evolution through heat treatment, Mater. Charact. 114 (2016) 62–74, https://doi.org/10.1016/j.matchar.2016.02.004.
[15] X. Wang, L.N. Carter, B. Pang, M.M. Attallah, M.H. Loretto, Microstructure and yield strength of SLM-fabricated CM247LC Ni-Superalloy, Acta Mater. 128 (2017) 87–95, https://doi.org/10.1016/j.actamat.2017.02.007.
[16] A. Singh, S. Nag, S. Chattopadhyay, Y. Ren, J. Tiley, G.B. Viswanathan, et al., Mechanisms related to different generations of γ′ precipitation during continuous cooling of a nickel base superalloy, Acta Mater. 61 (1) (2013) 280–293, https://doi.org/10.1016/j.actamat.2012.09.058.
[17] R. Radis, M. Schaffer, M. Albu, G. Kothleitner, P. Pölt, E. Kozeschnik, Multimodal size distributions of γ′ precipitates during continuous cooling of UDIMET 720 Li, Acta Mater. 57 (19) (2009) 5739–5747, https://doi.org/10.1016/j.actamat.2009.08.002.
[18] T. Rojhirunsakool, A. Singh, S. Nag, J.Y. Hwang, J. Tiley, R. Banerjee, Temporal evolution of non-equilibrium γ' precipitates in a rapidly quenched nickel base superalloy, Intermetallics 54 (2014) 218–224, https://doi.org/10.1016/j.intermet.2014.06.011.
[19] Y. Liu, S. Li, Y. Pei, H. Zhang, S. Gong, Precipitation of γ′ phases during slow cooling of nickel based superalloy, Mater. Res. Innov. 18 (sup4) (2014) S4-390–S4-394, https://doi.org/10.1179/1432891714Z.000000000708.
[20] F. Masoumi, D. Shahriari, M. Jahazi, J. Cormier, A. Devaux, Kinetics and Mechanisms of γ' Reprecipitation in a Ni-based Superalloy, Sci. Rep. 6 (2016) 28650, https://doi.org/10.1038/srep28650.
[21] A. Singh, S. Nag, J.Y. Hwang, G.B. Viswanathan, J. Tiley, R. Srinivasan, et al., Influence of cooling rate on the development of multiple generations of γ′ precipitates in a commercial nickel base superalloy, Mater. Charact. 62 (9) (2011) 878–886, https://doi.org/10.1016/j.matchar.2011.06.002.
[22] S.S. Babu, M.K. Miller, J.M. Vitek, S.A. David, Characterization of the microstructure evolution in a nickel base superalloy during continuous cooling conditions, Acta Mater. 49 (20) (2001) 4149–4160, https://doi.org/10.1016/S1359-6454(01)00314-7.
[23] X.P. Tan, D. Mangelinck, C. Perrin-Pellegrino, L. Rougier, C.-A. Gandin, A. Jacot, et al., Spinodal Decomposition Mechanism of γ′ Precipitation in a Single Crystal Ni-Based Superalloy, Met. Mat. Trans. A 45 (11) (2014) 4725–4730, https://doi.org/10.1007/s11661-014-2506-8.
[24] G.B. Viswanathan, R. Banerjee, A. Singh, S. Nag, J. Tiley, H.L. Fraser, Precipitation of ordered phases in metallic solid solutions: a synergistic clustering and ordering process, Scr. Mater. 65 (6) (2011) 485–488, https://doi.org/10.1016/j.scriptamat.2011.06.002.
[25] D.M. Collins, N. D'Souza, C. Panwisawas, C. Papadaki, G.D. West, A. Kostka, et al., Spinodal decomposition versus classical γ′ nucleation in a nickel-base superalloy powder: an in-situ neutron diffraction and atomic-scale analysis, Acta Mater. 200 (2020) 959–970, https://doi.org/10.1016/j.actamat.2020.09.055.
[26] A.S. Shaikh, M. Rashidi, K. Minet-Lallemand, E. Hryha, On as-built microstructure and necessity of solution treatment in additively manufactured Inconel 939, Powder Metall. 9 (1) (2022), https://doi.org/10.1080/00325899.2022.2041787.
[27] S. Sun, Q. Teng, Y. Xie, T. Liu, R. Ma, J. Bai, et al., Two-step heat treatment for laser powder bed fusion of a nickel-based superalloy with simultaneously enhanced tensile strength and ductility, Addit. Manuf. 46 (2021) 102168, https://doi.org/10.1016/j.addma.2021.102168.
[28] J. Xu, F. Schulz, R.L. Peng, E. Hryha, J. Moverare, Effect of heat treatment on the microstructure characteristics and microhardness of a novel γ′ nickel-based superalloy by laser powder bed fusion, Results Mater. 12 (2021) 100232, https://doi.org/10.1016/j.rinma.2021.100232.
[29] K. Lindgren, F. Schulz, H. Gruber, A. Markström, E. Hryha, On the role of Zr and B addition on solidification cracking of IN738LC produced by laser powder bed fusion, Materialia 26 (2022) 101609, https://doi.org/10.1016/j.mtla.2022.101609.
[30] M.K. Miller, R.G. Forbes, Atom-Probe Tomography: The Local Electrode Atom Probe, Springer, 2014.
[31] K. Lindgren, M. Bjurman, P. Efsing, M. Thuvander, Integrated effect of thermal ageing and low flux irradiation on microstructural evolution of the ferrite of welded austenitic stainless steels, J. Nucl. Mater. 551 (2021) 152967, https://doi.org/10.1016/j.jnucmat.2021.152967.
[32] J. Zhou, J. Odqvist, M. Thuvander, P. Hedström, Quantitative evaluation of spinodal decomposition in Fe-Cr by atom probe tomography and radial distribution function analysis, Microsc. Micro 19 (3) (2013) 665–675, https://doi.org/10.1017/S1431927613000470.
[33] INCO. Alloy IN-738 Technical Data: A Practical Guide to the use of Nickel-Containing Alloys No 497 2020.
[34] B. Wahlmann, F. Galgon, A. Stark, S. Gayer, N. Schell, P. Staron, et al., Growth and coarsening kinetics of gamma prime precipitates in CMSX-4 under simulated additive manufacturing conditions, Acta Mater. 180 (2019) 84–96, https://doi.org/10.1016/j.actamat.2019.08.049.
[35] F. Schulz, H.Y. Li, H. Kitaguchi, D. Child, S. Williams, P. Bowen, Influence of tertiary gamma prime (γ′) size evolution on dwell fatigue crack growth behavior in CG RR1000, Met. Mat. Trans. A 49 (9) (2018) 3874–3884, https://doi.org/10.1007/s11661-018-4779-9.